Photochemistry and Photobiology, 2020, 96: 388–396

Fluorescence and Treatment Light Monitoring for Interstitial Photodynamic Therapy†,‡

Christian Heckl*[1,2], Maximilian Aumiller[1,2], Adrian Rühm[1,2], Ronald Sroka[1,2] and Herbert Stepp[1,2]

[1]Laser-Forschungslabor, LIFE Center, University Hospital, LMU Munich, Munich, Germany
[2]Department of Urology, University Hospital, LMU Munich, Munich, Germany

Received 30 September 2019, revised 12 November 2019, accepted 21 November 2019, DOI: 10.1111/php.13203

ABSTRACT

In interstitial photodynamic therapy, light is distributed to the tumor via light diffusers. The light dose and the related phototoxic effect achieved throughout the target volume critically depend on absorption, scattering and diffuser positioning. Using liquid tissue phantoms, we investigated the dependencies of treatment light transmission and protoporphyrin IX (PpIX) fluorescence on these parameters. This enabled monitoring hemoglobin oxygenation and methemoglobin formation during irradiation (635 nm, 200 mW cm^{-1} diffuser length). Starting with two parallel cylindrical diffusers at 10 mm radial separation, the light transmitted between the fibers was largely determined by the minimal distance between the diffusers, but rather insensitive to an additional axial displacement or tilting of one fiber with respect to the other. For fixed distance between the diffusor centers, however, tilting up to direct contact resulted in a 10-fold signal increase. For hemoglobin within erythrocytes, irradiation leads to photobleaching of PpIX without marked change in hemoglobin oxygenation until hemolysis occurs. Afterward, hemoglobin is rapidly deoxygenized and methemoglobin is formed, leading to a dramatic increase in absorption. For lysed blood, these effects start immediately. A comparison of intraoperative monitoring of the signals with the experimental results might help prevent insufficient treatment by reconsidering treatment planning or prolonging irradiation.

INTRODUCTION

The 5-aminolevulinic acid (5-ALA) has obtained worldwide clinical approval as a prodrug of protoporphyrin IX (PpIX) for fluorescence-guided surgery (FGS) of malignant glioma—most recently by the FDA in USA (1). Numerous studies have shown that PpIX accumulation upon oral delivery of 5-ALA at a dose of 20 mg kg^{-1} bw 3–4 h prior to surgery is highly tumor-selective, summarized and discussed in (2,3). Especially, the positive predictive value (PPV) of visible PpIX fluorescence proved to be very high, reaching up to 100% in some clinical studies (4,5). A high PPV is of essential importance in brain tumor surgery because it excludes resection or treatment of the normal, functional brain. In other words: whatever brain tissue does show strong PpIX fluorescence contains tumor and can usually be resected without risking functional deficits. The Normal brain accumulates no or only minute amounts of PpIX (6).

The proven high tumor selectivity of PpIX accumulation stimulated a revival of experimental and clinical studies on photodynamic therapy (PDT) for malignant glioma (2,7–9). One of the two main approaches relies on performing fluorescence-guided surgery first and then irradiating the surgical cavity (9), whereas the other concept addresses predominantly inoperable or recurrent tumors by stereotactic interstitial irradiation (8). In this latter case, cylindrical diffuser fibers are inserted into the tumor after careful planning of appropriate trajectories, which exclude injuries of blood vessels and other critical structures but allow for distribution of a sufficient amount of light to the entire tumor volume.

A favorable feature of PpIX in this context is its fast photobleaching. Due to the irregular shape of malignant glioma, there is always a high probability that normal brain tissue receives rather high light doses even with very careful pretreatment planning. Fortunately, it was reported that the accumulation of PpIX in normal brain tissue, gray and white matter, is very low compared to the target brain tumor (10). Furthermore, it can be assumed that during illumination the little amount of PpIX accumulated in normal brain cells will be photobleached before a lethal amount of reactive oxygen species (ROS) is produced (8). This is an important inherent safety feature of 5-ALA-based interstitial PDT of malignant glioma, strongly relaxing light dosimetry considerations of this approach (8). However, a deeper clinical investigation on whether the potential therapeutic advantage is compromised by the observation that gray matter appears to be more sensitive to PDT-induced damage than tumor tissue would be desirable (10).

In order to monitor photobleaching during interstitial PDT, spectral online monitoring (SOM) was established to assess the average PpIX fluorescence in the tumor volume between adjacent treatment fibers at least prior to and after PDT irradiation (11,12). In addition to PpIX fluorescence, the treatment light transmission (at 635 nm) could be monitored between adjacent fibers. Only one of the cylindrical diffuser fibers was connected

*Corresponding author email: Christian.Heckl@med.lmu.de (Christian Heckl)
†This article is part of a Special Issue dedicated to Dr. Jarod Finlay.
‡This manuscript is part of the inaugural thesis of Christian Heckl to be submitted at the Medical Faculty of the Ludwig-Maximilians-Universität, Munich.

to the laser output port at a time for these measurements, while the other fibers were sequentially connected to a spectrometer and thus served as light detectors. The recorded spectra showed an intensity maximum at 635 nm and another one at 700 nm, corresponding to treatment light transmission and PpIX fluorescence, respectively. In order to account for the huge intensity differences of both signals, a long-pass filter was included in the detection beam path, rejecting most of the laser light.

Because tissue optical properties at the excitation wavelength of 635 nm and the emission wavelength of PpIX at around 700 nm are not identical, the interpretation of the acquired SOM-spectra is unfortunately not straightforward. However, it would be good, if one could at least roughly draw immediate conclusions from the acquired spectra: Whether the laser light transmission is in an acceptable range, or whether there is enough PpIX between fibers, where proliferating tumor tissue is expected. As the absolute intensities are strongly dependent on the distance, this may also be the case for the ratio of 700 nm PpIX fluorescence intensity *versus* 635 nm laser light transmission also. The primary aim of the present investigation is to experimentally assess the dependence of light signals measured between one pair of cylindrical diffuser fibers on the relative position and orientation of the fibers with respect to each other.

The intraoperative SOM measurements performed in (11,12) resulted in interesting and unexpected observations regarding the intensity and/or dynamics of the recorded transmitted laser light. For example, occasionally, the transmitted intensity dropped to undetectable levels after PDT. Such strong PDT-induced changes in optical tissue properties have only been reported a few other times: In a proceedings paper, Andrade *et al.* (13) reported about white light remission spectroscopy they had performed on 5-ALA treated normal mouse skin. In their investigation, PDT was more efficient in reducing oxygen saturation and generating methemoglobin (met-Hb) than radiotherapy. As deoxygenated hemoglobin (deoxy-Hb) and met-Hb have a significantly higher molar absorption at 635 nm than oxygenated hemoglobin (oxy-Hb), this observation translates into an increase of tissue absorption. Hamada *et al.* (14) had irradiated red blood cells dissolved in photosensitizer (talaporfin) solution and monitored absorption spectra during irradiation at a wavelength of 664 nm. Other than some hemolysis, they found the expected reduction in oxygen saturation and the formation of met-Hb. In an earlier investigation, Larsen *et al.* (15) had found met-Hb formation in a rat bladder tumor model, in which some of the animals the relative contribution to overall oxy-Hb was up to 40% after 5-ALA-based PDT. Interestingly, met-Hb has a broad absorption peak at ca. 630 nm, where oxy-Hb is far less absorbing (27 times less) and even deoxy-Hb absorbs about 3.5 times less (Fig. 3C). It is well known that ROS, for example, produced by photosensitizers, is able to oxidize hemoglobin to met-Hb (16) as is also with heating to above 60°C (17). If relevant amounts of deoxy-Hb and met-Hb were produced within the PDT treatment volume, this has consequences for light dosimetry because of spectral changes in absorption. Especially, for interstitial PDT, the formation of met-Hb during PDT may have a significant influence on overall tissue absorption and spatial light distribution at the treatment wavelength of 635 nm. If cylindrical diffuser fibers are several optical penetration depths apart from each other, the light transmission losses due to even moderate increase in absorption potentiate accordingly. It can be hypothesized that the occasionally observed loss of treatment light transmission between fibers after interstitial PDT with glioma patients (11) may therefore at least partly be caused by the ROS-induced formation of deoxy- and met-Hb. Therefore, it was the second aim of the present investigation to experimentally assess the dynamics of laser light transmission between one pair of cylindrical diffuser fibers while recording the spectral changes of white light transmission indicating changes in hemoglobin (oxy- *versus* deoxy- and met-Hb).

MATERIALS AND METHODS

Phantom preparation. To simulate the optical properties of biological tissue, liquid phantoms with India ink (29770, Rohrer & Klingner Leipzig-Co., Zella-Mehlis, Germany) or blood (see details below) as absorber, Lipovenös® (Lipovenös MCT 20%, Fresenius, Bad Homburg, Germany) as scatterer, Tween® 20 (P1379, Sigmar Aldrich, St. Louis, Missouri), Protoporphyrin IX (PpIX) (Protoporphyrin IX, Sigmar Aldrich) as fluorochrome and phosphate-buffered saline (PBS) (P5493, Sigmar Aldrich) as medium were prepared. The concentrations of the absorption medium and scattering medium were chosen to represent physiological absorption and scattering coefficients of the normal brain or brain tumor tissue at 635 nm (18–20). As base values, absorption and scattering coefficients $\mu_a = 0.02\ mm^{-1}$ and $\mu_s' = 2\ mm^{-1}$, respectively, were used. These values were previously measured intraoperatively for brain adjacent tumor tissue (20,21). Phantoms of varying absorber (India ink) concentrations from 0.025‰, 0.05‰, 0.1‰, 0.15‰ and 0.2‰ were created to represent a range of physiologically expected absorption coefficients μ_a of (0.02, 0.04, 0.07, 0.10, 0.14) mm^{-1}, respectively. By using India ink as absorber, a slightly lower absorption coefficient occurs at 700 nm of about 10% in comparison to the one at 635 nm. Additionally, different reduced scattering coefficients were simulated by different concentrations of Lipovenös®, varied from 1%, 1.5%, 2%, 2.5% and 3% representing $\mu s'$ of (1.2, 1.8, 2.3, 3.5, 4.6) mm^{-1}, respectively. The optical properties of the phantoms were measured using the integrating sphere technique as described by others (22). As a fluorochrome, PpIX powder was dissolved in DMSO at a concentration of 1 g L^{-1} to prepare a stock solution and further diluted with PBS to final sample concentrations of 10 or 20 μmol L^{-1}, which are reported as being physiological concentrations found in glioblastoma tissue after oral application of 20 mg kg^{-1} bw of 5-ALA (6). A concentration of 5 % Tween20 prevents aggregation of PpIX molecules, which would influence the measured transmission and fluorescence signals (23). The phantom was replenished with PBS.

For investigating the potential PDT-induced effects on hemoglobin, similar liquid phantoms, but with blood as absorber were prepared. Venous blood was taken from healthy volunteers (University Hospital LMU Munich ethics protocol: 18–144). The blood was either used immediately or stored in a refrigerator. Prior to adding blood to the liquid phantoms, it was centrifuged at 2500 rpm for 5 min (121 ***g***) and the supernatant (plasma) was removed. The sedimented erythrocytes were then either diluted the original volume with PBS to obtain a blood-equivalent with intact, but "washed" erythrocytes or with distilled water to obtain lysed blood. To remove all residual constituents except hemoglobin from the lysed blood sample, it was freeze-thawed, centrifuged and only the supernatant was used for further preparation. Scattering was adjusted to $\mu_s' = 2.3\ mm^{-1}$ at 635 nm by adjusting Lipovenös® to 2% final concentration. A blood concentration of 4% (corresponding to a μ_a of 0.03 mm^{-1} at 80% blood oxygenation) was chosen, and the PpIX concentration used was 20 μmol L^{-1}.

Measurement setup and fibers. A diode laser at 635 nm (Ceralas, Biolitec® AG, Vienna, Austria) was calibrated to emit 200 mW cm^{-1} from a 2 cm cylindrical light diffuser fiber (CD-4L3-20, LifePhotonics GmbH, Bonn, Germany). A second similar fiber was used as a detection fiber, which was connected to a spectrometer (USB2000+, OceanOptics, Largo, Fl) which incorporates a 657 nm long-pass filter. The long-pass filter did not completely block the transmitted laser light, thus enabled the recording of transmitted laser light and PpIX fluorescence simultaneously as is done during clinical iPDT (11).

Fluorescence and treatment light detection at different optical properties and fiber orientations. Clinically, the perfect fiber positioning is challenging, thus different orientations of the fibers with respect to

each other were investigated as shown in Fig. 1 which might support the interpretation of the measured transmitted treatment light and PpIX fluorescence signals. The fiber positions were investigated with respect to the distance between two parallel fibers (Fig. 1A), their relative axial positions (Fig. 1B), their angular deviation to the *y*-axis at the *y*-*z*-plane at the center of the diffuser tip (Fig. 1C) and the angular deviation to the *y*-axis at the *y*-*x*-plane (Fig. 1D) until the tips of the two fibers were in contact. To also evaluate the geometric dependence of the transmission and fluorescence signals on variable optical tissue properties, different concentrations of absorber and scatterer were investigated.

The distance between fibers in Fig. 1A was adjusted to 3, 4, 5, 6, 8, 10, 12, 14, 16, 18 and 20 mm from fiber center to fiber center. The axial displacement in Fig. 1B was investigated in 5 mm steps to a total displacement of 40 mm. Investigated angles were 0°, 5°, 10°, 20°, 45° and 90° in the configuration of Fig. 1C and 0°, 5°, 10°, 20° and 30° in the configuration of Fig. 1D. In the setups C and D, the distance d between the fibers in the middle of the light-emitting diffuser region area was kept at 10 mm.

Influence of blood absorption during PDT. The experimental setup as depicted in Fig. 1A with a constant interfiber distance of 10 mm was used. The volume of the liquid phantoms was 50 mL only, in order to limit the interaction volume between light and hemoglobin and the available content of PpIX in this volume, in an attempt to mimic the clinical situation. The phantom was stirred during the measurement at 200 min^{-1}.

During irradiation, white light transmission spectra were collected in regular intervals with a device, comprising a white light LED, a fiber bundle probe immersed into the phantom and a spectrometer (AvaSpec-Mini2048(CL), Avantes, Apeldoorn, The Netherlands). The fiber bundle consists of six excitation fibers surrounding a single detection fiber, all fibers having 400 µm cores. Before measuring the phantoms, a reference spectrum was collected from a phantom with all constituents except blood. Each measured spectrum was divided by the reference spectrum prior to storage.

During one of the experiments with washed erythrocytes, 2 mL of the liquid phantom were withdrawn prior to and at 15 min intervals after the start of irradiation. These samples were centrifuged (121 ***g***, 5 min) and 20 µL of the supernatant in the central fraction, containing the lowest concentration of sedimented erythrocytes (bottom fraction) and scattering lipid (top fraction) were extracted with a 10 µL pipette, diluted 1:100 with PBS and then measured in a cuvette absorption spectrometer (Lambda40, Perkin Elmer, Waltham, Massachusetts). No further measurements were performed to determine the degree of hemolysis of every single 20 µL sample derived in this way.

Data evaluation. The recorded spectra were evaluated using Matlab (R2018b, MathWorks, Natick, Massachusetts) and SigmaPlot (v11.0, Systat Software, Erkrath, Germany). Raw data spectra were averaged over wavelength intervals of 2 nm. All phantoms were prepared and measured in at least three independent replicates.

For the evaluation of the influence of blood absorption during iPDT, the spectra recorded from the detection fiber were evaluated as follows: a four pixel (2 nm interval) average was calculated for the intensities $I(\lambda)$ at wavelengths λ of 635 nm (laser light transmission), 674 nm (photoproduct (PP) fluorescence peak) and 700 nm (second PpIX fluorescence peak). As the fluorescence spectra $I_{PP}(\lambda)$ and $I_{PpIX}(\lambda)$ of PP and PpIX overlap, the pure signal contributions I_{PP}(674 nm) of PP at 674 nm and I_{PpIX}(700 nm) of PpIX at 700 nm were separated using Eqs. (1) and (2):

$$I_{PP}(674\text{nm}) = \left(I(674\text{nm}) - x_{PpIX} \cdot I(700\text{nm})\right/\left(1 - x_{PP} \cdot x_{PpIX}\right) \quad (1)$$

$$I_{PpIX}(700\text{nm}) = \left(I(700\,\text{nm}) - x_{PP} \cdot I(674\ \text{nm})\right)/\left(1 - x_{PP} \cdot x_{PpIX}\right) \quad (2)$$

where I_{PP}(674 nm) and I_{PpIX}(700 nm) are the signal intensities in counts per second that would have been recorded at 674 and 700 nm due to the fluorescence emission intensities of PP and PpIX without overlap, I (674 nm) and I(700 nm) are the counts per second actually measured on the examined phantoms at the respective wavelengths, and x_{PP} and x_{PpIX} are the ratios of the intensities emitted by pure PpIX at 674 and 700 nm and by pure PP at 700 and 674 nm, respectively. The values for x_{PP} and x_{PpIX} had been determined to x_{PP} = 0.65 and x_{PpIX} = 0.281 for the spectrometer in use.

The recorded white light transmission spectra were fitted with pure spectra of oxy-Hb, deoxy-Hb and met-Hb (as depicted in the results Fig. 3C) according to Eq (3). This equation calculates the relative contributions of oxy-Hb, deoxy-Hb and met-Hb to the measured spectrum.

$$I(\lambda) = I_0 \cdot \exp\left(-\left(a \cdot A_{oxy}(\lambda) + b \cdot A_{deoxy}(\lambda) + c \cdot A_{met}(\lambda)\right)\right) \quad (3)$$

where $I(\lambda)$ is the model function with fit parameters a, b and c representing the contributions of the absorption spectra of oxy-Hb (A_{oxy}), deoxy-Hb (A_{deoxy}) and met-Hb (A_{met}) to the measured spectrum. I_0 is another fit parameter, which is expected to be close to 1 because the measured spectra were scaled to the reference signal obtained on a phantom without absorber. Spectral ranges with the characteristic shapes of oxyhemoglobin (530–580 nm) and met-Hb (590–650 nm) were given higher weights (up to 30×) to obtain good fits (compare Fig. 3B). The weighing reduced the residuals of the difference of measured and fitted spectra, thus improving

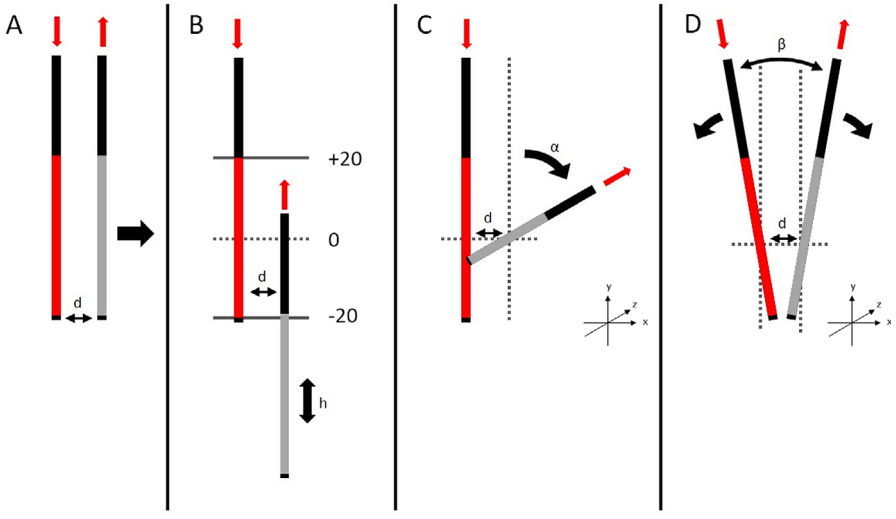

Figure 1. Positioning of the emitting and detecting fiber. The graph shows the light-guiding fibers in black, with the diffuser regions in red for the emitting fiber and gray as detecting fiber, respectively. The emitting and detecting fibers were placed parallel to each other at several distances (A) and in different relative axial positions (B), as indicated by the black arrows. A relative angular deviation within the *y*-*z*-plane (C) as well as within the common *y*-*x*-plane (until the tips of the fibers are in contact) (D) were applied to investigate the corresponding signal dependencies for nonparallel fiber pairs. The *x*-distances *d* of the centers of the diffuser regions in the experimental setups B, C and D were fixed at 10 mm.

the determination of the relative contributions of oxy-Hb, deoxy-Hb and met-Hb.

RESULTS

Fluorescence and treatment light detection at different optical properties and fiber orientations

Figure 2 shows the results of the experimental measurements of the assessment of light penetration at several fiber orientations at different optical properties. Each graph shows the mean value with a standard deviation of three measurements independently taken.

The transmission and fluorescence intensities in graph 2A and 2B are normalized to the measured intensities at 10 mm with an absorption coefficient of $\mu_a = 0.07$ mm^{-1} and a reduced scattering coefficient of $\mu_s' = 2.3$ mm^{-1} (blue line). As expected, the detected treatment light decreases roughly exponentially with increasing (radial) fiber distance. The decay becomes faster with increasing scattering (B) and in particular with increasing absorption (A). The detected fluorescence signals behavior similarly to the transmission signals, albeit with a generally slower decay.

The comparison of the fluorescence intensity and the transmission intensity is shown in Fig. 2C, where the fluorescence signals divided by the transmission signals are plotted at different distances between the emission and the detection fibers at an absorption coefficient of $\mu_a = 0.07$ mm^{-1} and a reduced scattering coefficient of $\mu_s' = 2.3$ mm^{-1}. With shorter distances between the two fibers, the fluorescence signal reaches 38% and 70.8% of the transmission intensity value at 5 and 8 mm, respectively.

The results of the investigation of two fibers at different relative axial positions are shown in Fig. 2D, geometry Fig. 1B. This measurement was implemented with one fixed absorption coefficient ($\mu_a = 0.07$ mm^{-1}) and one fixed scattering coefficient ($\mu_s' = 2.3$ mm^{-1}). The intensity increases while the detection fiber is pulled from below the emission fiber until the two fibers are parallel at the same height. Then, when the detection fiber is moved until its tip is at the level of the beginning of the diffused emission area of the emission fiber, the intensity decreases. The measured intensities are at the same level when the detection fiber is located above or below the light-emitting diffuser region of the emission fiber. In the region −10 mm to 10 mm, the deviation of the transmission intensity is less than 25%.

Fig. 2E shows the results where the detection fiber is tilted with respect to a y-axis in the y-z-plane, geometry Fig. 1C. It can be seen that with increasing the angular deviation the measured transmission intensity decreases by up to 39 %. At small angular deviations at about 10°, however, an intensity decrease of only 2.3% occurs.

In case, the fiber geometry was adjusted such that both fibers were tilted until their tips get in contact, geometry Fig. 1D, the results are shown in Fig. 2F. As the angular deviation increases, as the fiber tips approach, the measured transmission intensity increases by a factor of up to 14.3. At an angular deviation of 10°, an intensity increase occurs by a factor of 2.

Influence of blood absorption during PDT

Liquid phantom measurements with lysed blood or washed erythrocytes were performed to detect any PDT-induced changes in

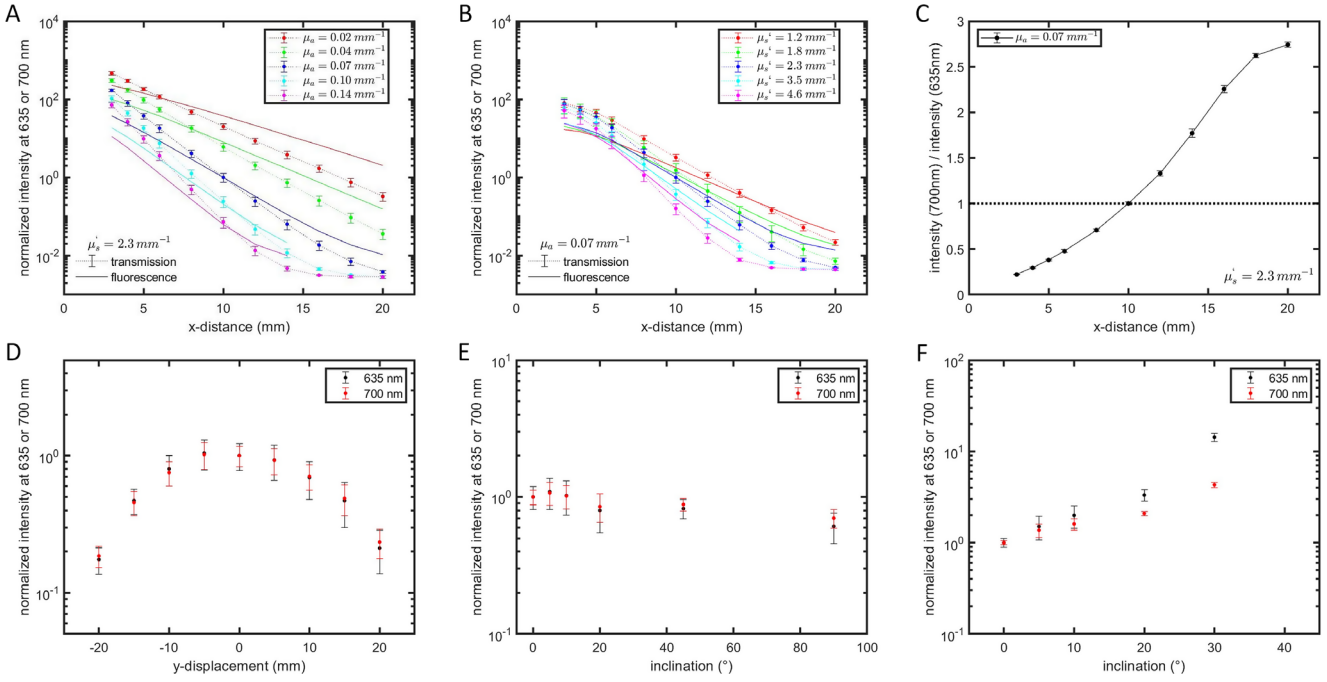

Figure 2. Results of interfiber light transmission and PpIX fluorescence measurements at different optical properties and different relative fiber positions. Each graph shows the normalized mean value at 635 nm for transmission and 700 nm for fluorescence at 10 mm fiber distance and at μ_a of 0.07 mm^{-1} and μ_s' of 2.3 mm^{-1} with a standard deviation of three independent measurements. Graph A and B show the decrease of treatment light transmission (dotted line) and fluorescence (solid line) intensities between two parallel fibers with increasing distance and with increasing absorption or reduced scattering coefficients, respectively. The distance-dependent ratio of the fluorescence and transmission signals is shown in graph C. Graph D shows the treatment light and fluorescence intensities at different relative axial positions of parallel fibers. The influence of out-of-common-plane and within-common-plane angular deviations (until the tips are in contact) are shown in graphs E and F, respectively.

absorption at the irradiation wavelength (635 nm), PpIX fluorescence (700 nm photobleaching), PP fluorescence (at 674 nm), oxy-, deoxy- and met-Hb. Spectra, as recorded by the cylindrical diffuser fiber serving as a detector, are shown in Fig. 3A. At the start of irradiation (black line), strong signals are observed, both for the laser light transmitted from the emission fiber to the detection fiber (635 nm) and the characteristic PpIX fluorescence generated within the tissue (peaking at 700 nm). During irradiation, an additional local maximum at 674 nm appears, while the PpIX fluorescence signal at 700 nm decreases. Interestingly, the transmitted laser light detected at 635 nm decreases as well, indicating increasing light absorption at 635 nm within the tissue, as the output of laser light from the irradiating diffuser remained constant throughout the experiment. The source of this increase in absorption becomes obvious from Fig. 3B: At the start of irradiation (black line), the white light transmission spectra show the imprint of mostly oxy-Hb. During irradiation, the contributions of deoxy-Hb and potentially met-Hb were detected (indicated by the additional minimum at around 635 nm after 60 min and verified by the local absorption maximum of met-Hb shown in Fig. 3C).

Figures 4 and 5 depict, the time-dependent signals of laser light transmission, PpIX and PP fluorescence (graph A), as well as the fit contributions (fit parameters a, b and c Eq. (3)) of oxy-, deoxy- and met-Hb (graph B). Figure 4 shows the results obtained for samples with lysed blood, while Fig. 5 shows the results for samples, where washed erythrocytes were added to the same final blood volume. In both cases, the absorption at 635 nm at the end of irradiation was much higher than at start, leading to a signal reduction by two orders of magnitude (black lines in the graphs A). The PpIX fluorescence signal was also decreasing with time. The signal decrease detected at 700 nm could be caused by an increase of absorption at the excitation and/or the emission wavelengths and/or by PpIX-photobleaching. Since the absorption changes could be caused by a variety of substances with different spectral characteristics, for example, different hemoglobin species, absorption and photobleaching effects could not be quantitatively separated from each other within our experimental approach. As visible in the green curve, photoproduct (PP) was formed shortly after the onset of irradiation. The related signal then decreased, potentially also due to photobleaching, together with the PpIX signal. In Figures 4 and 5, Graphs B show almost the same contributions of the different hemoglobin species at the start of irradiation. Also, in both cases deoxy-Hb increases at the cost of oxy-Hb, while fitted met-Hb was formed at a slower rate, but finally continues to increase at the cost of deoxy-Hb, leading to a maximum of the deoxy-Hb signal as soon as oxy-Hb had disappeared almost completely. The most striking differences between lysed blood (Fig. 4) and washed erythrocytes (Fig. 5) are threefold:

1 With lysed blood, there is an immediate onset of treatment light transmission reduction and deoxygenation of hemoglobin, while these signals stay relatively constant for a while in the case of washed erythrocytes, although PpIX is clearly photobleaching.
2 Less overall PP formation in the case of lysed blood.
3 An obviously steeper decrease of laser light transmission and related signals in the case of washed erythrocytes as soon as the initial "lag-phase" has passed.

Figure 6 indicates that when irradiating washed erythrocytes in the phantom experiment, the erythrocytes are destroyed at least partially, as evident by the characteristic hemoglobin absorption observed in the supernatant of centrifuged phantoms, which gets more and more pronounced with increasing irradiation time beforehand. Hemolysis seems to be largely completed already at 15 min after the start of irradiation, which is earlier than the onset of the fast absorption increase at 30–40 min as shown in Fig. 5A. However, the centrifugation did not separate the layers very clearly and withdrawing a clear layer without scattering was not possible. A quantitative interpretation of the absorption spectra is therefore not possible.

DISCUSSION

Fluorescence and treatment light detection at different optical properties and fiber orientations

The investigations of different fiber arrangements demonstrated a moderate dependence on axial displacements and angular

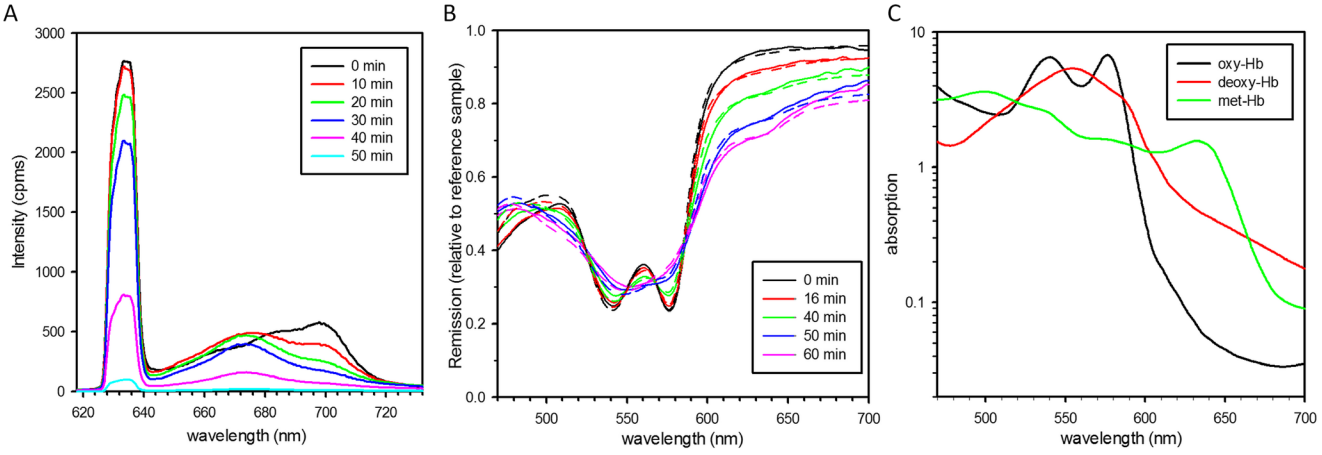

Figure 3. Graph A: Time-dependent spectral changes as measured with a spectrometer connected to the detecting fiber after low pass filter. Sample with washed erythrocytes. The Peak at 635 nm: treatment light transmission, peak at 700 nm: PpIX fluorescence, peak at 674 nm: PP fluorescence. Graph B: Time-dependent white light transmission spectra with respect to a nonabsorbing reference sample (solid lines). Sample with lysed blood. Dashed lines: the result of curve fit according to Eq. (3). Graph C: Blood absorption spectra used for fitting.

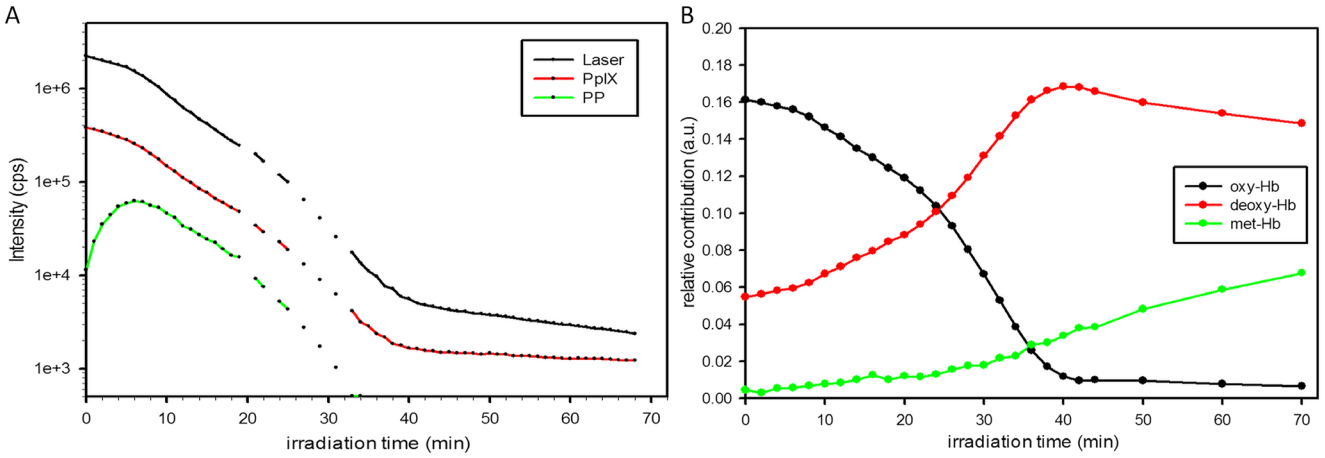

Figure 4. Results of experiments with lysed blood. Graph A: Time-dependent signals of transmitted treatment light (black line), PpIX fluorescence (red line) and PP fluorescence (green line). Graph B: Time-dependent fit parameters for the contributions of oxy-Hb (black line), deoxy-Hb (red line) and met-Hb (green line).

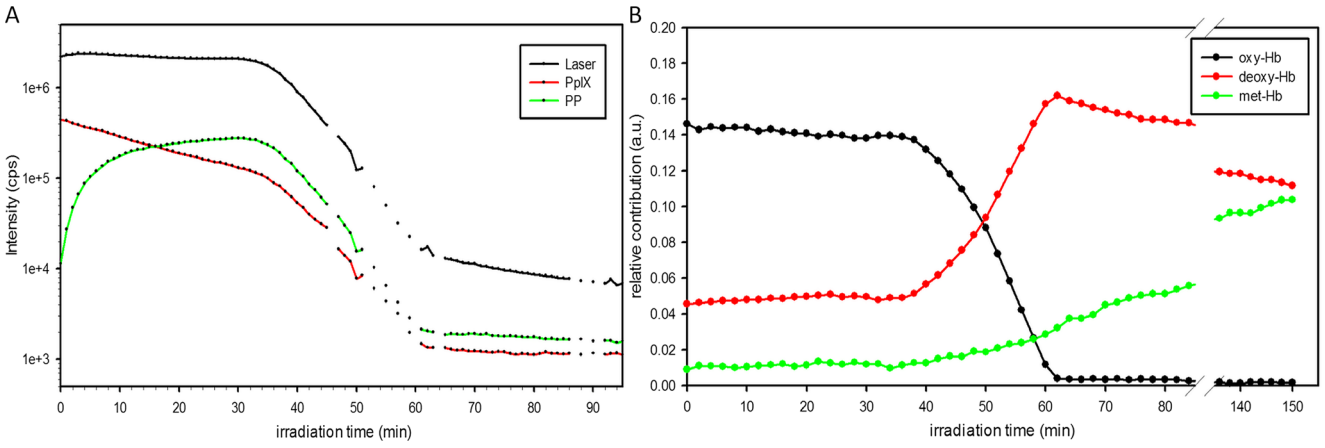

Figure 5. Results of experiments with washed erythrocytes. Graph A: Time-dependent signals of transmitted treatment light (black line), PpIX fluorescence (red line) and PP fluorescence (green line). Graph B: Time-dependent fit parameters for the contributions of oxy-Hb (black line), deoxy-Hb (red line) and met-Hb (green line).

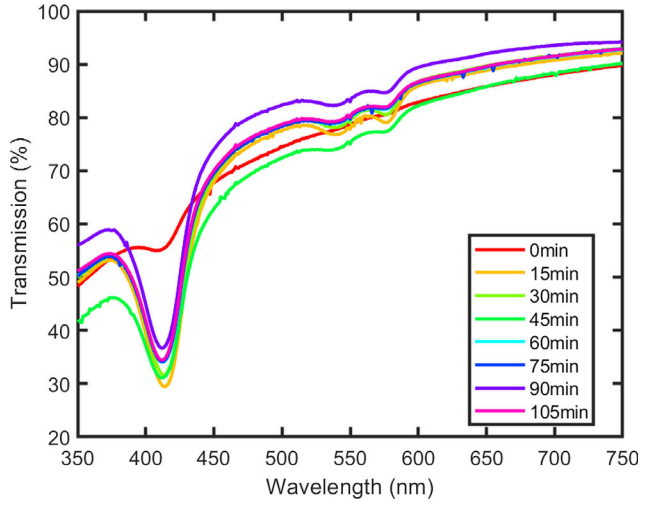

Figure 6. Transmission spectra of the transparent component of centrifuged samples from phantoms with washed erythrocytes prior to and at different times after the start of irradiation.

deviations within the *y*-*z*-plane, while the signal increases more than 10-fold if the fiber tips get in contact due to angular deviation within the *y*-*x*-plane. This should be kept in mind during treatment planning. Of course, it will always be intended to plan the fiber trajectories as parallel to each other as possible, but the location of vulnerable structures and larger blood vessels frequently require some deviation from this strategy. It becomes obvious that unavoidable angular deviations should be implemented under careful consideration of the relative positions of adjacent fibers. Fortunately, none of these deviations from the treatment plan lead to a signal decrease by more than a factor of 2, as long as the shortest distance between the fibers is close to 10 mm. The strong signal increase resulting from angular deviations within the *y*-*x*-plane (Fig. 2F) would not impede PDT as long as dose-volume histograms indicate sufficient tumor coverage, but it could produce undue tissue heating and should, therefore, be avoided.

The slopes of the distance-dependent fluorescence signals (Fig. 2A,B) are considerably less steep than the slopes of the corresponding treatment light transmission signals. This is due to

the somewhat lower absorption and scattering at the emission wavelength compared to the excitation wavelength. As a consequence, both signals decrease with increasing distance, but the fluorescence intensity less so than the transmitted treatment light. Fig. 2C, clearly indicates the ratio of the corresponding peak heights detected for parallel diffusers and the parameter combination μ_a of 0.07 mm^{-1} and μ_s' of 2.3 mm^{-1}, normalized to 1 for the used "standard conditions" at 10 mm separation.

A closer look at the μ_s' variations of the distance-dependent signals in Fig. 2B (at a fixed absorption) shows converging curves at a shorter distance and even crossovers. This is to be expected, as multiple scatter may return light from larger distances, an effect which also leads to increased light intensities underneath the tissue surface if scatter dominates absorption (24).

Provided the fiber-based signal detection is carefully calibrated, Fig. 2A,B allow deducing the expected absolute signal intensities for a given interfiber distance for both the laser light transmission and the PpIX fluorescence. As the curves are rather steep, the interfiber distance has to be known precisely to draw quantitative conclusions: an uncertainty of 1 mm can lead to a 2-fold higher or lower intensity. On the other hand, a significantly higher absorption than planned has an even stronger influence on the measured signals. If the treatment planning was done with assuming $\mu_a = 0.02$ mm^{-1} for instance, but in fact was $\mu_a = 0.07$ mm^{-1}, fluorescence and treatment light signals are reduced by a factor of 20–40 (at 10 mm fiber distance). If the transmission signal is significantly (about 10-fold) lower than expected, the suspicion of having induced some capillary bleeding may be justified. Lilge *et al.* (10,25) reported to local changes in the tissue optical properties following iPDT for intracranial VX2 tumors, referring to local hemorrhage around fiber tips, vasodilatation, vasoconstriction and small changes in blood content in the tissue as possible explanations. The fibers concerned should then be given treatment light as soon as possible to minimize the loss of PDT efficiency by blood absorption and hemoglobin transformation. A final judgment of the relevance of such assumptions will be possible, as soon as sufficient clinical data are available.

In interstitial photodynamic therapy of brain tumors, several cylindrical diffuser fibers are placed into the tumor (11). For all fiber pairs, transmission and fluorescence measurements can be performed and the average optical tissue parameters and PpIX fluorescence can be calculated. For this evaluation, knowledge of the 3D coordinates of the fiber trajectories are required. If such spectral measurements are performed before the start of irradiation, the information can be used to adjust light dosimetry and thus to perform a patient individualized therapy. A similar approach has previously been described by Finlay *et al.* (26) for iPDT of the prostate, where isotropic emitters and detectors are moved along the trajectories within transparent catheters. The authors could measure the photosensitizer concentration by recording absorption spectra because the photosensitizer used has a higher absorption at longer wavelengths (MLu absorbs at 735 nm). This is not a realistic option for PpIX, but the fluorescence at 700 nm can easily be detected and when the tolerable range of signal intensities prior to and after PDT (then reduced via photobleaching) is known, appropriate conclusions may be drawn, for example, to prolong irradiation, if photobleaching is not achieved to a sufficient degree.

Influence of blood absorption during PDT

During interstitial PDT of malignant glioma, it was previously observed that the transmission of laser light at 635 nm between adjacent cylindrical diffuser fibers (ca. 10 mm apart) usually stays constant over the 1 h irradiation time with 200 mW cm^{-1} diffuser length (11). But there are also cases, where a gradual decrease in laser light transmission between fibers could be observed. Sometimes there was hardly any signal detectable after PDT. One may speculate that during insertion of the diffuser fibers into the tumor, some capillaries may be ruptured and cause some bleeding around the fiber tips. However, a continuous whole blood layer would have to become more than 300 μm thick in order to explain a 90% loss of transmission (27). An equivalent signal loss would be induced by an increase in blood volume–fraction in the entire tissue, for example, from 4% to about 11%, as obtained from calculations for a point source, diffusion approximation and $\mu_a = 0.02$ mm^{-1} and $\mu_s' = 2$ mm^{-1}, which corresponds reasonably well with Fig. 2A. A similar trend could be induced by an oxygenation of hemoglobin within the treated volume. Such an effect has, in fact, been claimed as indicated in the introduction (14,15) and attributed to the interaction of a photosensitizer with hemoglobin, which leads to the formation of deoxy-Hb and met-Hb at the cost of initially dominating oxy-Hb. Finlay *et al.* also (26) reported on a PDT-induced increase of deoxy-Hb detected by white light absorption spectroscopy. Met-Hb can also be induced by heating to above 60°C. We could exclude thermal met-Hb formation in our experimental conditions by detecting no changes in Hb signals at all if PpIX was not added to the phantom (data not shown).

Under "regular" conditions during PpIX-based iPDT, the photosensitizer PpIX inside the tumor cells is well separated from the hemoglobin inside erythrocytes traveling in blood vessels. In addition, as long as there is perfusion, there will always be new, well-oxygenated, hemoglobin continuously replacing any deoxy-Hb. If there is some interstitial bleeding, however, such erythrocytes might potentially remain in the treatment region and some extracellular PpIX might then interact with these erythrocytes. Our experiments with washed erythrocytes are in accordance with the assumption that as long as the hemoglobin is well packed in erythrocytes, there is little to no access of singlet oxygen to the hemoglobin in the erythrocytes. Transmission stays rather stable. Meanwhile, PpIX is clearly undergoing some photobleaching, obviously consuming oxygen dissolved in the surrounding. It takes considerable time (at least 20 min under our experimental conditions) to allow the photosensitizer sufficient access to the hemoglobin. Extracts of the sample clearly show ongoing hemolysis at this time (Fig. 6). Interestingly, once the erythrocytes are destroyed, the hemoglobin deoxygenation occurs at a rate at least as fast as in the case of lysed blood. This is astonishing because the PpIX has already been photobleached to below 20% at this time. The only plausible explanation for this observation we can think of is that most of the dissolved oxygen has been used up at this time, and the further generation of singlet oxygen is then restricted to the conversion of oxygen bound in hemoglobin, seeing a steeper O_2 gradient. In two other independent experiments on hemoglobin samples using the same procedure, the obtained composition parameters showed a very similar behavior in each case (see Supporting Information, Figs. S1 and S2). Only the time after which singlet oxygen

in the erythrocytes receives access to hemoglobin varies between 20 and 40 min among the experiments.

The observation of PDT-induced formation of deoxy-Hb and met-Hb in optical tissue phantoms with blood may have very relevant clinical implications. If the mechanical insult on the brain tumor tissue during insertion of the light diffuser fibers induces some hemorrhage, tissue absorption may not only increase due to the increased blood volume fraction but also by the formation of much stronger absorbing deoxy-Hb and met-Hb during the subsequent irradiation. As a consequence, one should aim for minimizing the time delay between fiber insertion and the start of irradiation. This minimizes both effects. Monitoring of the laser light transmission between light diffusers before and after irradiation provides valuable information on whether and how severely tissue absorption may have increased. A systematic recording of such events for multiple patients should finally clarify the relative contributions of an increase in blood volume fraction and PDT-induced effects to increases in tissue absorption. If an intracavity PDT is to be performed after tumor resection, it must be ensured before starting the irradiation that as little blood as possible is present on the cavity walls because potentially similar conversion processes can be induced during irradiation. One should mention that tissue hypoxia might also lead to increased absorption due to an increased proportion of deoxy-Hb with implications for treatment efficacy (28).

The fits of pure hemoglobin spectra to the measured white light transmission spectra were of limited quality. One possible reason is the probe geometry, which does not allow for recording well-controlled, plain absorption or transmission spectra. The average light path length will vary with absorption, underestimating stronger absorption due to a reduction in effective path length. This deficit might be minimized by applying a more elaborate analysis, for example, as presented by Finlay and Foster in (29). However, the qualitative differences between lysed blood and intact erythrocytes would not change. Here, we were not interested in quantifying blood oxygen saturation in untreated tissue, but in identifying any PDT-induced changes in hemoglobin absorption at 635 nm. Another reason is the relatively restricted emission bandwidth of the white light LED with rather limited intensities at short and long wavelengths. The absolute values of the contributions of the different hemoglobin species should therefore not be overinterpreted in a quantitative manner.

The validity of the phantom experiments is limited, as vital biological tissue may be discussed as follows: In vital tissue, photosensitizer and hemoglobin are well separated, which was also the case in half of the comparative phantom experiments. The liquid phantom samples were prepared in 50 ml containers and were gently stirred continuously. This volume is considerably larger than the typically irradiated tissue volume during iPDT (4–8 mL per fiber). On the other hand, in vital tissue, the blood fraction within the tissue is connected to blood vessels and is therefore continuously exchanged, which means that it will not take part in the dynamic PDT-induced effects. Only hemorrhage will lead to amounts of blood resting in a certain tissue region, starting from very low blood volume fractions, while in the phantoms the blood volume fraction is constant and recruited from the same 50 ml volume over the full observation time. These differences may partly compensate each other in terms of the time-dependent signal evolution. Another difference is the exposure to PpIX. In our experiments, PpIX was added shortly before the start of irradiation. Still, there were a few minutes of "drug light interval" and may have led to the different lag times of erythrocyte destruction observed in Fig. 5. If PpIX had some time to diffuse into erythrocytes, the time to onset of hemoglobin transformation may be shorter. It is unknown, how much of extracellular PpIX is present in viable glioblastoma tissue. In any case, the sooner irradiation starts after insertion of the fibers, the less the risk of early hemoglobin transformation, absorption increase and insufficient treatment.

We are confident that the phantom experiments are realistic enough to point out a possibly important phenomenon to be considered for iPDT. The details of the kinetics of the onset and speed of hemoglobin deoxygenation and met-Hb formation may be different, but that it can occur in case of hemorrhage and that it can vary significantly alter the light distribution and thus affect the therapeutic irradiation should be well considered, and the effect should be monitored intraoperatively.

In summary, this manuscript shows:

1 Light transmission between cylindrical diffuser fibers as investigated in this work did not strongly depend on relative fiber positions or orientations as long as the minimal distance between the diffusor regions remained unchanged.
2 As fluorescence light undergoes less absorption and scattering than treatment light, the relative intensity of the PpIX fluorescence signal increases with increasing distance.
3 PDT can induce deoxygenation and met-Hb formation in immobilized blood (after hemorrhage for example), which strongly increases the absorption at 635 nm. This may contribute to the clinically observed occasional loss of treatment light transmission between adjacent diffuser fibers during PDT.

Acknowledgement—We would like to thank Ahmed Saleh (German University Cairo) for his support in carrying out the experimental measurements. Financial support from photodynamic GmbH & Co. KG and support from DFG Graduiertenkolleg GRK 2274 are gratefully acknowledged.

SUPPORTING INFORMATION

Additional supporting information may be found online in the Supporting Information section at the end of the article:

Figure S1. Results of independent replicates with lysed erythrocytes to the results of Figure 4 of the main publication. In the two left graphs, the time-dependent signals of transmitted treatment light (black lines), PpIX fluorescence (red line) and PP fluorescence (green line) are depicted. The right graphs show the time-dependent fit parameters for the contributions of oxy-Hb (black line), deoxy-Hb (red line) and met-Hb (green line).

Figure S2. Results of independent replicates with washed erythrocytes to the results of Figure 5 of the main publication. In the two left graphs, the time-dependent signals of transmitted treatment light (black lines), PpIX fluorescence (red line) and PP fluorescence (green line) are depicted. The right graphs show the time-dependent fit parameters for the contributions of oxy-Hb (black line), deoxy-Hb (red line) and met-Hb (green line).

REFERENCES

1. FDA. Aminolevulinic acid hydrochloride, known as ALA HCl (Gleolan, NX Development Corp.) as an optical imaging agent indicated

in patients with gliomas. Available at: https://www.fda.gov/Drugs/InformationOnDrugs/ApprovedDrugs/ucm562645.htm2017.
2. Stepp, H. and W. Stummer (2018) 5-ALA in the management of malignant glioma. *Lasers Surg. Med.* **50**(5), 399–419.
3. Lakomkin, N. and C. G. Hadjipanayis (2018) Fluorescence-guided surgery for high-grade gliomas. *J. Surg. Oncol.* **118**(2), 356–361.
4. Stummer, W., J. C. Tonn, C. Goetz, W. Ullrich, H. Stepp, A. Bink, T. Pietsch and U. Pichlmeier (2014) 5-Aminolevulinic acid-derived tumor fluorescence: the diagnostic accuracy of visible fluorescence qualities as corroborated by spectrometry and histology and postoperative imaging. *Neurosurgery* **74**(3), 310–319.
5. Diez, Valle R., S. Tejada Solis, M. A. Idoate Gastearena, R. Garcia de Eulate, P. Dominguez Echavarri and J. Aristu Mendiroz (2011) Surgery guided by 5-aminolevulinic fluorescence in glioblastoma: volumetric analysis of extent of resection in single-center experience. *J. Neurooncol.* **102**(1), 105–113.
6. Johansson, A., G. Palte, O. Schnell, J. C. Tonn, J. Herms and H. Stepp (2010) 5-Aminolevulinic acid-induced protoporphyrin IX levels in tissue of human malignant brain tumors. *Photochem. Photobiol.* **86**(6), 1373–1378.
7. Mahmoudi, K., K. L. Garvey, A. Bouras, G. Cramer, H. Stepp, J. G. Jesu Raj, D. Bozec, T. M. Busch and C. G. Hadjipanayis (2019) 5-aminolevulinic acid photodynamic therapy for the treatment of high-grade gliomas. *J. Neurooncol.* **141**(3), 595–607.
8. Johansson, A., F. W. Kreth, W. Stummer and H. Stepp (2010) Interstitial photodynamic therapy of brain tumors. *IEEE J. Sel. Top. Quantum Electron.* **16**(4), 841–853.
9. Dupont, C., M. Vermandel, H. A. Leroy, M. Quidet, F. Lecomte, N. Delhem, S. Mordon and N. Reyns (2019) INtraoperative photoDYnamic Therapy for GliOblastomas (INDYGO): Study Protocol for a Phase I Clinical Trial. *Neurosurgery* **84**(6), E414–E419.
10. Lilge, L. and B. C. Wilson (1998) Photodynamic therapy of intracranial tissues: a preclinical comparative study of four different photosensitizers. *J Clin. Laser Med. Surg.* **16**(2), 81–91.
11. Rühm, A., H. Stepp, W. Beyer, G. Hennig, T. Pongratz, R. Sroka, O. Schnell, J. C. Tonn and F. W. Kreth (2014) 5-ALA based photodynamic management of glioblastoma. *Proc. SPIE* **8928**, 89280E.
12. Johansson, A., F. Faber, G. Kniebuhler, H. Stepp, R. Sroka, R. Egensperger, W. Beyer and F. W. Kreth (2013) Protoporphyrin IX fluorescence and photobleaching during interstitial photodynamic therapy of malignant gliomas for early treatment prognosis. *Lasers Surg. Med.* **45**(4), 225–234.
13. Andrade, C. T., M. S. Nogueira, S. C. Kanick, K. Marra, J. Gunn, J. Andreozzi, K. Samkoe, C. Kurachi and B. W. Pogue (2016) Optical spectroscopy of radiotherapy and photodynamic therapy responses in normal rat skin shows vascular breakdown products. Optical methods for tumor treatment and detection: mechanisms and techniques in photodynamic therapy XXV. *Proc. SPIE* **9694**, 969410.
14. Hamada, R., E. Ogawa and T. Arai (2019) Continuous optical monitoring of red blood cells during a photosensitization reaction. *Photobiomodul. Photomed. Laser Surg.* **37**(2), 110–116.
15. Larsen, E. L., L. L. Randeberg, O. A. Gederaas, C. J. Arum, A. Hjelde, C. M. Zhao, D. Chen, H. E. Krokan and L. O. Svaasand (2008) Monitoring of hexyl 5-aminolevulinate-induced photodynamic therapy in rat bladder cancer by optical spectroscopy. *J Biomed Opt.* **13**(4), 044031.
16. Hasselbalch, K. A. (1909) Untersuchungen ueber die Wirkung des Lichtes auf Blutfarbstoffe und rote Blutkoerperchen wie auch ueber optische Sensibilisation fuer die Lichtwirkung. *Biochem. Zeitschr.* **xix**, 435.
17. Randeberg, L. L., J. H. Bonesronning, M. Dalaker, J. S. Nelson and L. O. Svaasand (2004) Methemoglobin formation during laser induced photothermolysis of vascular skin lesions. *Lasers Surg. Med.* **34**(5), 414–419.
18. Gebhart, S. C., W. C. Lin and A. Mahadevan-Jansen (2006) In vitro determination of normal and neoplastic human brain tissue optical properties using inverse adding-doubling. *Phys. Med. Biol.* **51**(8), 2011–2027.
19. Yaroslavsky, A. N., P. C. Schulze, I. V. Yaroslavsky, R. Schober, F. Ulrich and H. J. Schwarzmaier (2002) Optical properties of selected native and coagulated human brain tissues in vitro in the visible and near infrared spectral range. *Phys. Med. Biol.* **47**(12), 2059–2073.
20. Beck, T. J., W. Beyer, T. Pongratz, W. Stummer, R. Waidelich, H. Stepp, S. Wagner and R. Baumgartner (2003) Clinical determination of tissue optical properties in vivo by spatially resolved reflectance measurements. *Photon Migration Diffuse Light Imag.* **5138**, 96–105.
21. Beck, T. J., F. W. Kreth, W. Beyer, J. H. Mehrkens, A. Obermeier, H. Stepp, W. Stummer and R. Baumgartner (2007) Interstitial photodynamic therapy of nonresectable malignant glioma recurrences using 5-aminolevulinic acid induced protoporphyrin IX. *Lasers Surg. Med.* **39**(5), 386–393.
22. Eisel, M., S. Ströbl, T. Pongratz, H. Stepp, A. Rühm and R. Sroka (2018) Investigation of optical properties of dissected and homogenized biological tissue. *J. Biomed. Opt.* **23**(9), 1–9.
23. Marois, M., J. Bravo, S. C. Davis and S. C. Kanick (2016) Characterization and standardization of tissue-simulating protoporphyrin IX optical phantoms. *J. Biomed. Opt.* **21**(3), 35003.
24. Jacques, S. L. (2010) How tissue optics affect dosimetry of photodynamic therapy. *J. Biomed. Opt.* **15**(5), 051608.
25. Lilge, L., M. Sepers, J. Park, C. O'Carroll, P. Pournazari, J. Prosper and B. C. Wilson (1997) Preclinical studies of photodynamic therapy of intracranial tissues. *Proc. SPIE* **2972**, 64–73.
26. Finlay, J. C., T. C. Zhu, A. Dimofte, D. Stripp, S. B. Malkowicz, R. Whittington, J. Miles, E. Glatstein and S. M. Hahn (2014) In vivo determination of the absorption and scattering spectra of the human prostate during photodynamic therapy. *Proc. SPIE* **5315**, 132–142.
27. Markwardt, N. A., N. Haj-Hosseini, B. Hollnburger, H. Stepp, P. Zelenkov and A. Rühm (2016) 405 nm versus 633 nm for protoporphyrin IX excitation in fluorescence-guided stereotactic biopsy of brain tumors. *J. Biophotonics* **9**(9), 901–912.
28. Ahn, P. H., J. C. Finlay, S. M. Gallagher-Colombo, H. Quon, B. W. Jr O'Malley, G. S. Weinstein, A. Chalian, K. Malloy, T. Sollecito, M. Greenberg, C. B. 2nd Simone, S. McNulty, A. Lin, T. C. Zhu, V. Livolsi, M. Feldman, R. Mick, K. A. Cengel and T. M. Busch (2018) Lesion oxygenation associates with clinical outcomes in premalignant and early stage head and neck tumors treated on a phase 1 trial of photodynamic therapy. *Photodiagnosis Photodyn. Ther.* **21**, 28–35.
29. Finlay, J. C. and T. H. Foster (2004) Hemoglobin oxygen saturations in phantoms and in vivo from measurements of steady-state diffuse reflectance at a single, short source-detector separation. *Med. Phys.* **31**(7), 1949–1959.